Reevaluation of the ^{22}Ne$(p, \gamma)^{23}$Na reaction rate

Sk Mustak Ali,[1,*] Rajkumar Santra,[2,†] Sathi Sharma,[3] and Ashok Kumar Mondal[3]
[1]*Facility for Rare Isotope Beams, Michigan State University, East Lansing, Michigan 48824, USA*
[2]*Variable Energy Cyclotron Centre, 1/AF, Bidhan Nagar, Kolkata 700064, India*
[3]*Department of Physics, Manipal University, Jaipur, Rajasthan 303007, India*

(Received 30 October 2023; revised 28 February 2024; accepted 28 March 2024; published 16 April 2024)

The ^{22}Ne$(p, \gamma)^{23}$Na capture reaction is a key step in the Ne-Na cycle of hydrogen burning. The rate of this reaction is critical in classical novae nucleosynthesis and hot bottom burning (HBB) processes in asymptotic giant branch (AGB) stars. Despite its astrophysical importance, significant uncertainty remains in the reaction rate due to several narrow low-energy resonances lying within and near the Gamow window. The present work revisits this reaction by examining the contribution of the 8664 keV subthreshold state and the 8945 keV doublet resonance state of $7/2^-$ configuration in ^{23}Na. Finite range distorted-wave Born approximation (FRDWBA) analysis of existing ^{22}Ne(^{3}He, d)^{23}Na transfer reaction data was carried out to extract the peripheral asymptotic normalization coefficients (ANCs) of the 8664 keV state. The ANC value obtained in the present work is ≈25% higher compared to the previous work by Santra *et al.* [Phys. Rev. C **101**, 025802 (2020)]. Systematic R-matrix calculations were performed to obtain the nonresonant astrophysical S factor utilizing the enhanced ANC value. The resonance strengths of the 8945 keV doublets were deduced from shell model calculations. The rate calculations are performed by omitting the resonances at E_x = 8862, 8894, and 9000 keV, which are unlikely to exist as reported by Carrasco-Rojas *et al.* [Phys. Rev. C **108**, 045802 (2023)]. The total reaction rate is found to be ≈15–20% higher at temperatures relevant for the HBB processes, compared to the recent rate measured by Williams *et al.* [Phys. Rev. C **102**, 035801 (2020)], and matches their rate at temperatures of interest for classical novae nucleosynthesis.

DOI: 10.1103/PhysRevC.109.045809

I. INTRODUCTION

The neon-sodium (Ne-Na) cycle is of enormous importance in stellar nucleosynthesis as it is responsible for the hydrogen burning in massive stars, and is involved in the synthesis of elements between Ne and Mg [1,2]. Within the Ne-Na cycle, the proton capture reaction ^{22}Ne$(p, \gamma)^{23}$Na ($Q = 8794.11 \pm 0.02$ keV) is of significant interest. It not only consumes ^{22}Ne, which is the third most abundant nuclide produced in stellar helium burning, but also produces ^{23}Na, the only stable isotope of sodium [3,4]. This reaction influences the weak s-process nucleosynthesis by competing with the ^{22}Ne$(\alpha, n)^{25}$Mg reaction, which is a major neutron source in asymptotic giant branch (AGB) stars. The rate of this reaction impacts the stellar models that seek to explain the puzzling anticorrelation in oxygen and sodium abundances observed in globular clusters [5,6]. It affects the abundance ratios of Ne isotopes in presolar grains extracted from meteorites [7]. Further, sensitivity studies have shown that the nuclear uncertainties of the ^{22}Ne$(p, \gamma)^{23}$Na reaction can have a drastic impact on the ^{22}Ne and ^{23}Na abundances in classical novae nucleosynthesis [8]. The reaction rate of ^{22}Ne$(p, \gamma)^{23}$Na at astrophysical energies depends on the contribution of several low energy resonances in ^{23}Na (Fig. 1) and a slowly varying nonresonant capture component. The uncertainty in the rate spanned a factor of 1000 between the rates from NACRE [10] and others [11–13]. This discrepancy was addressed by direct measurements by the LUNA Collaboration [14], where they measured the strengths of three new resonances at $E_x(E_{\text{c.m.}}) = 8945(151)$, 8972(178), and 9042(248) keV [15–17] and proposed new stringent upper limits for 8862(68) and 8894(100) keV resonances [18]. The nonresonant S factor was also measured at unprecedentedly low energies (proton energies E_p = 188–310 keV) to study the contributions of direct capture (DC) and the subthreshold resonance at 8664 keV [18]. Kelly *et al.* [19] confirmed the existence of the 8945(151) and 8972(178) keV resonances along with measuring the strength of the 9211(417) keV resonance relative to the 9252(458) keV resonance. Recently, Williams *et al.* [7,20] carried out the first inverse kinematics measurement of the ^{22}Ne$(p, \gamma)^{23}$Na reaction at TRIUMF. They measured a total of seven resonances from 8945(151) to 10016(1222) keV. Interestingly, they reported a significantly lower strength for the 9252(458) keV resonance compared to Kelly *et al.* [19]. Their rate was four times higher than the rate from the STARLIB-2013 nuclear reaction-rate library[13] at $T = 0.1$ GK ($T_9 = 0.1$). The impact of this new rate on the isotopic abundances in carbon-oxygen

*mustak@frib.msu.edu
†Corresponding author: rajkumarsantra2013@gmail.com; Present address: Department of Physics, University of Calcutta, Kolkata 700009, India.

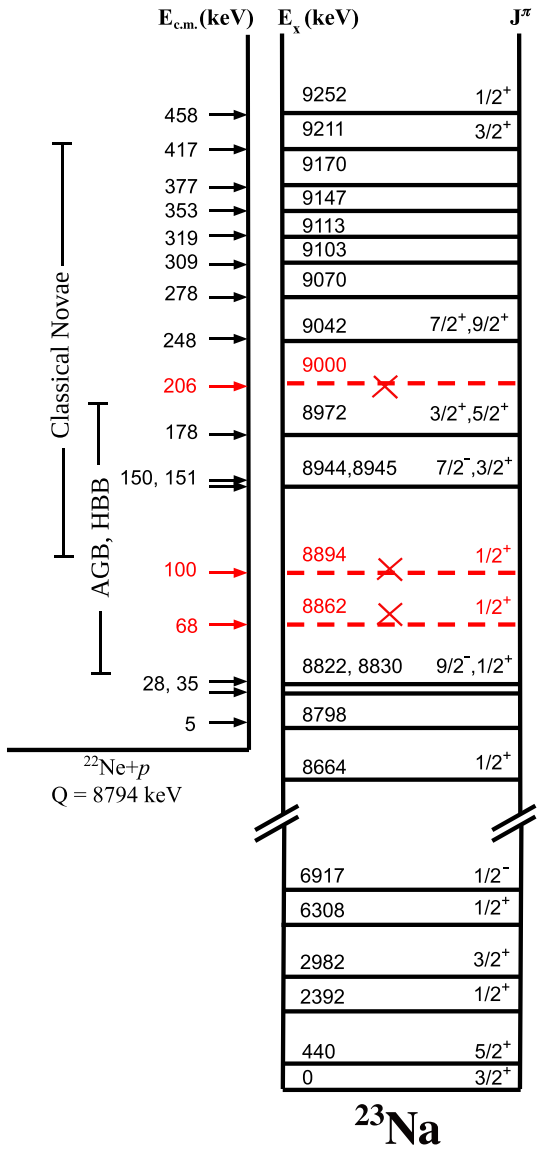

FIG. 1. Energy level diagram of ^{23}Na depicting resonances in the ^{22}Ne $+p$ system relevant for different astrophysical scenarios. The three tentative resonances at $E_x = 8862$, 8894, and 9000 keV that are unlikely to exist [9] are shown in red.

(CO) and oxygen-neon (ONe) novae ejecta was investigated. More than 10% change in the isotopic abundance within the Ne-Al region was observed for CO novae and a factor of 2 reduction in ^{22}Ne for ONe novae. Further, it was seen that the production of ^{23}Na is minimally influenced in AGB stars due to this new rate [7,20].

Despite these major improvements, contentions remain on the resonance strengths and the existence of some of the low energy resonances lying inside and near the Gamow window. The resonance at $E_x = 8945$ keV in ^{23}Na lies $\approx$150 keV above the proton threshold. It affects the ^{22}Ne$(p,\gamma)^{23}$Na reaction rate since it lies within the Gamow window at $T_9 = 0.1$. Previous measurements of the 8945 keV resonance considered it as a single state with $J^\pi = 7/2^-$ [11,21]. However, the measurement by Jenkins *et al.* [22] with Gammasphere reported that this resonance actually comprises a doublet, one member with $J^\pi = 7/2^-$ and the other with a tentative $J^\pi = 3/2^+$. Several direct measurements have obtained the resonance strength for the $3/2^+$ state, and the value ranges from 1.48×10^{-7} eV to 2.2×10^{-7} eV [16–20]. But no such direct measurements exist for the $7/2^-$ state, and an upper limit of 9.2×10^{-9} eV was recommended for its strength from the $(^3\text{He}, d)$ transfer reaction [11]. This strength was calculated from the spectroscopic factor for the 8945 keV state, assuming $l = 3$ transfer, consistent with $J^\pi = 7/2^-$. However, this assumption is questionable due to the limited number of data points in the angular distribution of the 8945 keV state. Subsequently, Kelly *et al.* [19] proposed an upper limit of 9.7×10^{-8} eV for the $7/2^-$ state. Recently, Santra *et al.* [23] reanalyzed the data of Hale *et al.* [11] considering the contribution of both the $3/2^+$ ($l = 2$ transfer) and $7/2^-$ ($l = 3$ transfer) states, extracting the spectroscopic factors for both the states. In their indirect study of the ^{22}Ne$(p,\gamma)^{23}$Na reaction, they carried out a systematic R-matrix analysis of the DC component, including the contribution of the 8664 keV state. The low energy behavior of the nonresonant S factor is controlled by this subthreshold resonance [18]. In Ref. [23], the R-matrix calculations were constrained by the asymptotic normalization coefficients (ANCs) extracted from the ^{20}Ne$(^3\text{He}, d)^{23}$Na transfer data at 15 MeV [24] for the first six bound states and 20 MeV [11] for the 8664 keV state. However, the ANC value of 144 fm$^{-1/2}$ obtained for the 8664 keV state in Ref. [23] did not satisfy the necessary peripherality conditions. The resulting S factor using this ANC value could not reproduce the DC $\rightarrow$ 8664 keV capture data at low energies, particularly for $E_p < 500$ keV. A better fit to the data was obtained by simultaneous R-matrix fit to the DC data of Rolfs *et al.* [2], Gorres *et al.* [21], and Ferraro *et al.* [18] with an ANC value of 166 fm $^{-1/2}$. The rate calculations in Ref. [23] included the contributions of the resonances at $E_x = 8862$, 8894, and 9000 keV. A recent measurement by Carrasco-Rojas *et al.* [9] concluded that these resonances are unlikely to exist (Fig. 1) and their contributions should be discarded from the rate calculations.

In the present work, we attempt to reexamine the ^{22}Ne$(p,\gamma)^{23}$Na reaction by focusing on the extraction of the peripheral ANC of the 8664 keV state. The angular distribution data of the ^{20}Ne$(^3\text{He}, d)^{23}$Na one-proton stripping reaction at energy of 15 MeV [24] is used to obtain the corresponding ANC and its peripheral nature is checked. Also, the contributions of the excited states 7080, 7449, and 7890 keV which were not considered in the previous analysis [23] are included in the present work. As discussed earlier, the spectroscopic factor for the $7/2^-$ configuration of the 8945 keV state still remains elusive of direct measurements. Hence, detailed microscopic shell model calculations are performed to yield the required proton width (Γ_p) and the corresponding resonance strength for this state. The rate calculations are carried out by omitting the three tentative resonances as suggested by Carrasco-Rojas *et al.* [9]. The resultant reaction rate as a function of temperature is

TABLE I. Potential parameters used in the present work. V and W are the real and imaginary depths in MeV; r and a are the radius and diffuseness in fm. $R_x = r_x A^{1/3}$ fm ($x = V, W, S, SO, C$).

Channel	V	r_V	a_V	W_V	r_W	a_W	W_S	r_S	a_S	V_{SO}	r_{SO}	a_{SO}	r_C	Ref.
^{22}Ne + ^{3}He	177.0	1.14	0.72	13.0	1.60	0.77				8.0	1.14	0.72	1.40	[24]
$d + ^{23}$Na	105.0	1.02	0.86				80.0	1.42	0.65	6.0	1.02	0.86	1.30	[24]
$d + ^{22}$Ne	88.0	1.17	0.73	0.24	1.33	0.73	35.8	1.33	0.73	13.85	1.07	0.66	1.33	[23]
$d + p$	[a]	1.25	0.65							6.2	1.25	0.65	1.30	[23]
$p + ^{22}$Ne	[a]	1.26	0.60							6.2	1.26	0.60	1.33	[23]

[a]Varied to match separation energy.

compared with the recent measurement and evaluation by Williams *et al.* [20].

II. ANALYSIS

A. Finite-range DWBA analysis and ANC extraction

Finite-range distorted wave Born approximation (FRDWBA) calculations were performed for the 8664 keV ($1/2^+$) subthreshold state in ^{23}Na using the existing angular distribution data of the ^{22}Ne(^{3}He, d)^{23}Na reaction at bombarding energy of 15 MeV [24]. An uncertainty of 10% is taken into account due to the digitization of data. The FRDWBA calculations required the optical model potential (OMP) parameters for the entrance channel ^{22}Ne + ^{3}He, exit channel $d + ^{23}$Na, and the core-core ^{22}Ne + d interactions. The real binding potentials for the $(d + p)$ and ^{22}Ne + p systems were also included, with their depths adjusted to reproduce the effective proton separation energy. The potentials were of the standard Woods-Saxon shape. The potential parameters are listed in Table I. The code FRESCO [25] was used to carry out the calculations. The resultant DWBA calculations along with the data are shown in Fig. 2. The proton spectroscopic factor S, was extracted by normalizing the calculated DWBA calculations to the experimental data,

$$\left(\frac{d\sigma}{d\Omega}\right)_{\text{Exp}} = S\left(\frac{d\sigma}{d\Omega}\right)_{\text{DWBA}}. \quad (1)$$

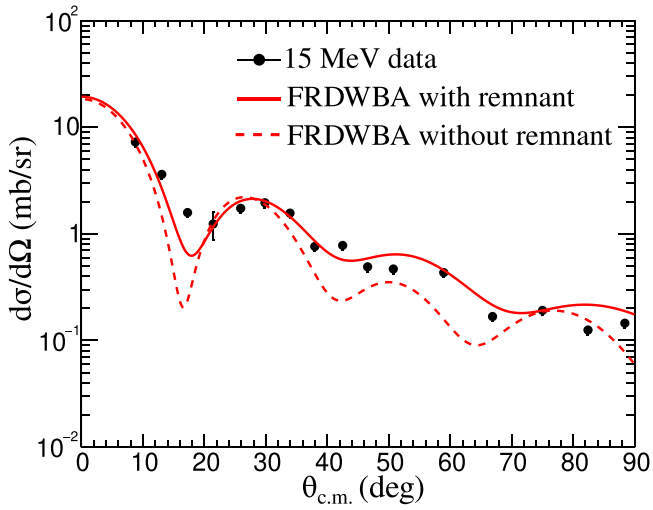

FIG. 2. Angular distributions of the 8664 keV state from the ^{22}Ne(^{3}He, d)^{23}Na reaction at 15 MeV [24]. The FRDWBA calculations are shown by the solid and dotted lines.

The spectroscopic factor for ^{3}He in $(d + p)$ configuration is taken as 1.16 [26]. The proton spectroscopic factor for the 8664 keV state from the present calculations is relatively higher than those obtained in Ref. [24,27] (Table II). Note that in these previous works, the zero-range DWBA calculations were used to explain the experimental data [24,27]. The inclusion of the complex remnant term in the present FRDWBA calculations results in a better overall fit to the data, as also seen by Ref. [23]. The dotted lines in Fig. 2 represent the FRDWBA calculation sans the remnant term. As discussed in Ref. [23], the spectroscopic factors are dependent on the choice of potential parameters and are sensitive to the geometric parameters of the bound state potentials. Thus, instead of spectroscopic factor, the ANC is a more appropriate quantity. The ANC method is free from the geometrical parameters of the binding potentials and relies primarily on the peripheral nature of the reaction. The square of the ANC (C^2) of a particular state is related to the spectroscopic factor (S) via the single particle ANC (b) as

$$C^2 = Sb^2. \quad (2)$$

The single particle ANC (b) is the normalization of the bound state wave function of the composite nucleus ^{23}Na at large radii with respect to the Whittaker function. To test the peripheral condition, the variation of the spectroscopic factor (S) against the single particle ANC (b) was studied for the 15 MeV data as shown in Fig. 3(a). The single particle ANC (b) is varied by changing the geometrical parameters of the ^{22}Ne + p binding potential in small steps. According to Eq. (2), the variation of S should be proportional to the inverse square of b. From Fig. 3(a), the S obtained from the 15 MeV data follows the inverse square relation. Hence, the ANC extracted from the 15 MeV data is peripheral and this ANC is considered for all further calculations. In Fig. 3(b), the extracted ANC is plotted as a function of b. The mean ANC obtained is 179.5 fm$^{-1/2}$ and is shown with the dotted line. In Fig. 4, the dependence of the ANC as a function of binding energy for the 8664 keV state is shown. The binding energy for the 8664 keV is 130 ± 3 keV [23]. It is varied by keeping the geometry parameters of the bound state potential fixed ($r_0 = 1.26$ fm, $a_0 = 0.60$ fm) corresponding to the mean ANC value. The plots show that the ANC value of the 8664 keV

TABLE II. Spectroscopic factors (S) and ANC (C) of E_x = 7080, 7449, 7890, and 8664 keV states of ^{23}Na from the present work.

E_x (keV)	J^π	nl_j	S (Present)	S (Literature)	b (fm$^{-1/2}$) (Present)	C (fm$^{-1/2}$) (Present)	C (fm$^{-1/2}$) (Literature)
8664	$1/2^+$	$2s_{1/2}$	0.50 ± 0.05	0.32 ± 0.05 [23] 0.58 ± 0.08 [28] 0.42 ± 0.08 [18] 0.30 [21] 0.29 [11] 0.31 [27] 0.27 [24]	249	179.5 ± 19.7	143.7 ± 15.2 [23]
7080	$1/2^-$	$2p_{1/2}$	0.08 ± 0.01	0.3 [27] 0.085 [24]	8.95	2.53 ± 0.16	
7449	$3/2^+$	$1d_{3/2}$	0.06 ± 0.01	0.28 [27] 0.14 [24]	3.93	0.96 ± 0.06	
7890	$3/2^+$	$1d_{3/2}$	0.05 ± 0.01	0.15 [27] 0.11 [24]	3.75	0.84 ± 0.08	

subthreshold state decreases with increasing binding energy. The ANC value for the 8664 keV state from the present work is ≈25% higher compared to that in Ref. [23].

The uncertainty of the mean value of ANC has contributions from two sources. The first one arises due to the propagation of the error of spectroscopic factors (S) through the relation given in Eq. (2). The errors in the values of S include the uncertainty of experimental angular distribution data. Second, the contribution of the uncertainty in binding energy is added in quadrature to obtain the total uncertainty in the mean ANC value. The dotted lines in Fig. 4 show the variation in ANC due to the ±3 keV uncertainty in the binding energy of the 8664 keV state.

Similar analyses were carried out to obtain the ANC values for the 7080, 7449, and 7890 keV states using the 15 MeV data which were not considered in the earlier work by Santra *et al.* [23]. The extracted spectroscopic factors and ANCs from the present work along with the values available in the literature are listed in Table II.

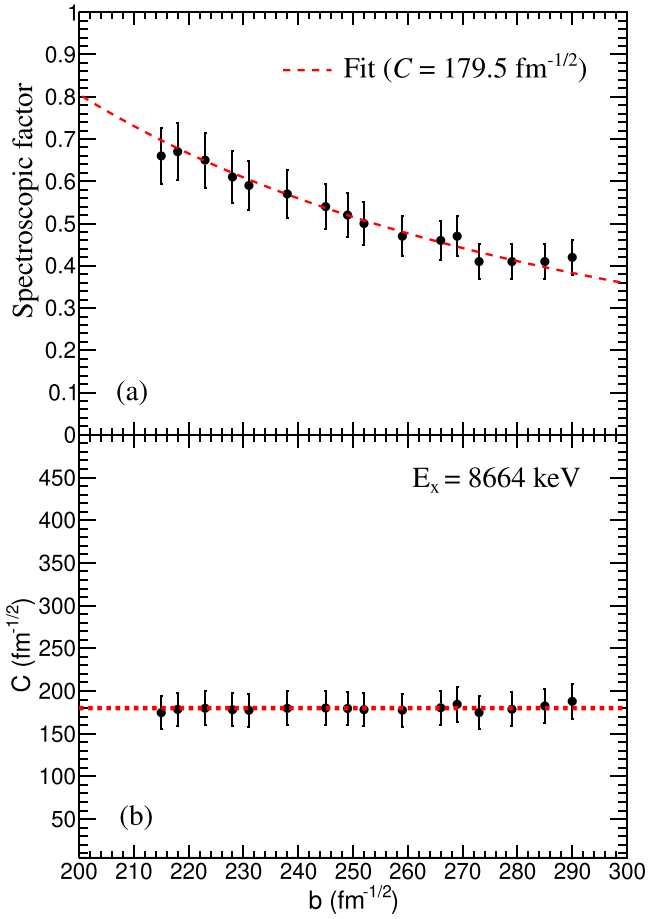

FIG. 3. (a) Variation of spectroscopic factor (S) with single particle ANC (b) for the 8664 keV state. (b) Variation of ANC (C) with single particle ANC (b) for the 8664 keV state.

B. *R*-matrix calculations

In the present work, a phenomenological R-matrix analysis was performed using the code AZURE2 [29]. The basic R-matrix theory used in the code AZURE2 is described in

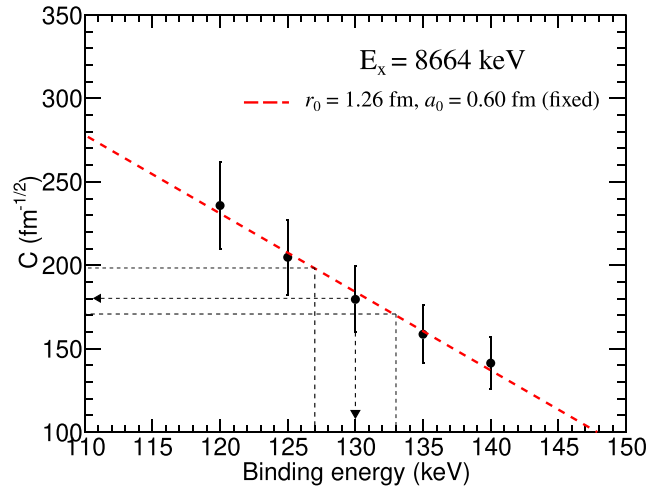

FIG. 4. Variation of ANC (C) with binding energy for the 8664 keV state.

TABLE III. Background pole parameters obtained from *R*-matrix fits.

			$\Gamma_\gamma[E_1]$ (eV)						
J^π	E_x (MeV)	Γ_p (MeV)	$R \to$ GS	$R \to 0.44$	$R \to 2.39$	$R \to 2.98$	$R \to 6.30$	$R \to 6.91$	$R \to 8.66$
$1/2^-$	15	5.0	822.91		3.17×10^3	697.67	1.58×10^3		139.528
$3/2^-$	15	5.0	20.92	974.42					

Ref. [29,30]. The *R*-matrix calculations were performed by introducing the channel radius (r_c) which divides the radial space into internal and external parts. The ANC determines the magnitude of the external capture cross section whereas the internal capture contribution is simulated by the high-energy background poles. Hence, the total nonresonant capture cross section contribution is modeled by the sum of the external and internal capture components. For the present calculations, $r_c = 5.3$ fm, is obtained for the ^{22}Ne $+p$ system by chi-square minimization procedure employing a grid search technique. The search is performed on the total nonresonant *S*-factor data by keeping the ANC values of the bound states and the decay width (Γ_γ) of 8664 keV state as fixed but varying the poles' parameters.

The *R*-matrix fitting has been performed on the available capture data of individual states and total nonresonance capture data simultaneously. The ANCs for the ground and the first five bound excited states were taken from Santra *et al.* [23]. For the three bound excited states at 7080, 7449, 7890 keV, and for the 8664 keV subthreshold state, the ANC values are taken from this work (Table II). For the internal capture part, two background poles with spin-parity $1/2^-$ and $3/2^-$ are included, and only the $E1$ decay was considered. The excitation energies of the poles are chosen at 15 MeV and proton partial widths are fixed at 5 MeV, calculated from Wigner limit approximations. However, the γ-decay partial widths of the background poles are left as free parameters, with the initial values taken from the Weisskopf limit for the corresponding γ transitions. The fitted background pole parameters are shown in Table III.

In order to see the effect of the enhanced ANC of the 8664 keV state, first the *R*-matrix calculations for the DC $\to$ 8664 keV transition are discussed. The resultant *S* factor and the differential *S* factor at $\theta = 90^\circ$ obtained using the mean peripheral ANC of 179.5 fm$^{-1/2}$ are shown with the red dotted lines in Figs. 5(a) and 5(b), respectively. The red band corresponds to the error in *S* factor due to the uncertainties in the ANC value and decay width (Γ_γ) of the 8664 keV state. The *S* factor obtained by including the peripheral ANC from this work is able to explain the DC $\to$ 8664 keV capture data by Gorres *et al.* [21] (open black triangles) within the uncertainty band as shown in Figs. 5(a) and 5(b). In Ref. [23], the authors obtained a better fit to the data of Gorres *et al.* [21] with a lower ANC value of 166 fm$^{-1/2}$. However, the present calculations could better explain the data by Kelly *et al.* [19] (filled blue circle) at $E_p = 425$ keV, within the uncertainty band compared to Ref. [23] as shown in Fig 5(a). The data points by Rolfs *et al.* [2] (filled black squares) at higher energies, lie above the upper limit of the *S*-factor band. The black dashed lines in Figs. 5(a) and 5(b) represent the external capture contribution.

The 8664 keV state has a lifetime of 0.14 ± 0.03 fs and it decays to the ground state (GS) with a branching of $(84 \pm 3)\%$ ($\Gamma_\gamma = 4.7 \pm 1$ eV) [21]. The DC $\to$ GS transition is influenced by the high energy tail of this *s*-wave subthreshold resonance ($E_p = -130$ keV), as is evident from the rise in the low energy *S*-factor data of Gorres *et al.* [21] and Ferraro *et al.* [18] (red squares) in Fig. 6(a). The corresponding *S* factors for the DC $\to$ GS transition from the *R*-matrix calculations

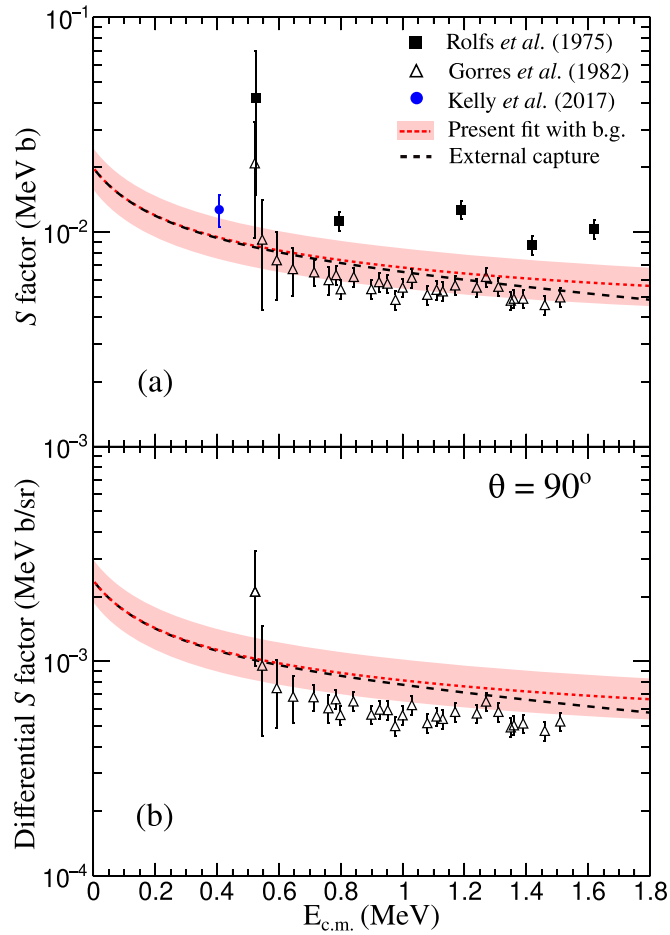

FIG. 5. (a) Astrophysical *S* factor and (b) differential *S* factor at $\theta = 90^\circ$, obtained from the *R*-matrix calculations for the DC $\to$ 8664 keV transition. The red dotted line corresponds to the *S* factor using the mean ANC of 179.5 fm$^{-1/2}$ for the 8664 keV state (b.g. represents background poles). The black dashed lines represent the external capture contribution. The bands correspond to the uncertainty in the *S* factor (see text for details).

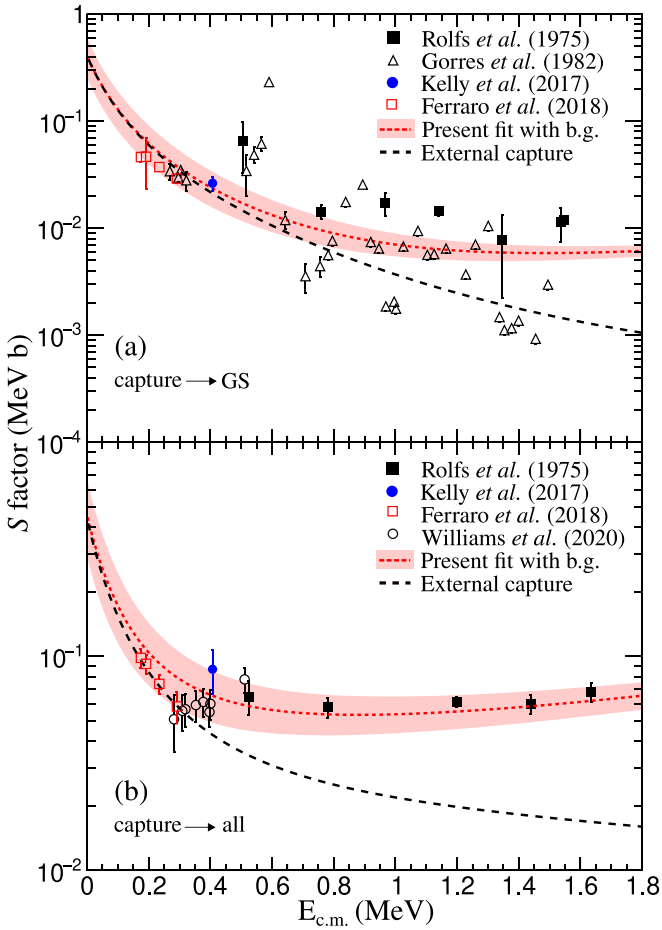

FIG. 6. Astrophysical S factor of the nonresonant capture in ^{22}Ne$(p,\gamma)^{23}$Na from previous direct measurements [2,18–21] and present R-matrix calculations. (a) Capture to the ground state in ^{23}Na. (b) Total S factor (b.g. represents background poles). The black dashed lines represent the external capture contribution. The bands correspond to the uncertainty in the S factor (see text for details).

are shown with the red dotted lines in Fig. 6(a). The calculations are in very good agreement with the low energy data ($E_{\text{c.m.}} < 400$ keV) of Gorres *et al.* [21]. The data of Ferraro *et al.* [18] and Kelly *et al.* [19] lie inside the uncertainty band. At higher energies, the calculated S factor passes through the data points of Gorres *et al.* [21] but underestimates the data of Rolfs *et al.* [2]. The rising nature of the S factor at low energies is very well reproduced by the calculations.

The total S factor for the nonresonant capture in ^{22}Ne$(p,\gamma)^{23}$Na reaction is obtained by adding the S factors of all the individual transitions to the ground and the bound excited states, and is shown with the red dotted line in Fig. 6(b). The calculations were carried out by including the ANCs for the three bound excited states 7080, 7449, and 7890 keV and the 8664 keV subthreshold state obtained from this work (Table II). The ANCs for the ground and the first five bound excited states were taken from Ref. [23]. The black dashed lines in Figs. 6(a) and 6(b) represent the external capture contribution. The uncertainties in the nonresonant S factors from the R-matrix calculations are due to the uncertainties in the ANC values and uncertainty in the decay width of the 8664 keV subthreshold state. The red-colored bands in Figs. 5 and 6 correspond to the resultant uncertainties in the calculated S factors. The upper (lower) part of the band is due to the upper (lower) error limits of the respective values. The total nonresonant S factor from the calculations is in agreement with the recent direct measurement data of Williams *et al.* [20] as well as with the lower energy data of Ferraro *et al.* [18].

C. Shell model calculations and partial widths for the 8945 keV resonance

The extraction of spectroscopic factors for the 8945 keV doublet by Hale *et al.* [11] and Santra *et al.* [23] are not completely reliable due to the scarce angular distribution data. In this work, the proton spectroscopic factor for the $7/2^-$ state of ^{23}Na at 8945 keV was calculated using the NUSHELLX code [31]. Large basis shell model (LBSM) calculations were performed. The positive parity states were easily reproduced using the *sd* model space. But, for the negative parity state, the upper *pf* shell was taken with the *sd* shell. Thus, the *sdpf* model space was used for the negative parity states. In this model space core is $N = Z = 8$, i.e., ^{16}O. The valence space consists of $1d_{5/2}$, $1d_{3/2}$, $2s_{1/2}$, $1f_{7/2}$, $1f_{5/2}$, $2p_{3/2}$, and $2p_{1/2}$ with single particle energies -3.948, 1.647, -3.163, 5.063, 10.022, 1.184, and 1.903 MeV respectively. The full model space calculation is constrained due to the present computational capacity. Hence, a suitable truncation scheme was adopted. In this scheme, the $1f_{5/2}$ subshell is kept unrestricted with zero occupancy in the $2p_{1/2}$ orbital. As the $7/2^-$ and $3/2^+$ doublet states are around 9 MeV, the higher single particle orbital plays an important role in reproducing the energies of the 8945 keV doublet. The SDPF-MU interaction [32] with the mentioned truncation scheme reproduces the observed $7/2^-$ state in ^{23}Na at 9820 keV. The calculated energy level is 875 keV above the experimentally adopted energy level. Similarly, the $3/2^+$ doublet state has been reproduced theoretically at 9998 keV. The proton spectroscopic factor for the $7/2^-$ state from the shell model calculations is 7.8×10^{-3} and for $3/2^+$ it is 1.6×10^{-3}. The shell model values are higher compared to the spectroscopic factors obtained in Refs. [11,23]. However, as discussed earlier the proton spectroscopic factors in Refs. [11,23] are debatable since the angular distribution has only three data points. To validate the theoretical calculations, the spectroscopic factors for the low-lying states of ^{23}Na were also calculated and compared with the corresponding experimental values, as shown in Table IV. The theoretical calculations are in good agreement with the experimentally determined values for these low lying states.

The proton partial widths (Γ_p) for the 8945 keV doublet are obtained using the relation

$$\Gamma_p = S\Gamma_{\text{sp}}, \tag{3}$$

where Γ_{sp} is the single particle width of resonance for pure single particle configuration calculated from the code DWUCK4 [33] and S is the spectroscopic factor from shell model calculations. The values of Γ_{sp} for the $3/2^+$ and $7/2^-$ states are 1.8×10^{-4} eV and 2.49×10^{-6} eV respectively. The partial γ-decay widths (Γ_γ) for $M1$ and $E1$ transitions

TABLE IV. Comparison of spectroscopic factors (S) for the low-lying bound states and the 8945 keV doublet states of ^{23}Na from the present shell model calculations ($S^{\rm SM}$) and literature.

E_x (keV)	J^π	nl_j	$S^{\rm SM}$ (This work)	S (Literature)
GS	$3/2^+$	$1d_{3/2}$	0.055	0.08 [24] 0.082 ± 0.012 [23]
440	$5/2^+$	$1d_{5/2}$	0.41	0.35 [24] 0.38 ± 0.08 [23]
2392	$1/2^+$	$2s_{1/2}$	0.20	0.25 [24] 0.26 ± 0.05 [23]
2982	$3/2^+$	$1d_{3/2}$	0.23	0.32 [24] 0.35 ± 0.04 [23]
6308	$1/2^+$	$2s_{1/2}$	0.10	0.13 [24] 0.14 ± 0.02 [23]
8945	$3/2^+$	$1d_{3/2}$	1.6×10^{-3}	$(5.54 \pm 1.41) \times 10^{-4}$ [23] 8.32×10^{-4} [11]
8944	$7/2^-$	$1f_{7/2}$	7.8×10^{-3}	$(3.94 \pm 0.9) \times 10^{-4}$ [23] $\leqslant 1.08 \times 10^{-3}$ [11]

obtained from the Weisskopf estimates [34] are 0.37 and 133.62 eV, respectively. The $7/2^-$ state of the 8945 keV doublet undergoes decay to $9/2^-$ and $9/2^+$ states emitting γ rays with energies (multipolarities) 2592 keV ($M1$) and 6240 keV ($E1$), respectively [22].

III. THERMONUCLEAR REACTION RATE OF ^{22}Ne$(p,\gamma)^{23}$Na

The thermonuclear reaction rate of the ^{22}Ne$(p,\gamma)^{23}$Na reaction is governed by various low energy narrow resonances and the nonresonant component. As there are no interfering resonances to consider for the ^{22}Ne$(p,\gamma)^{23}$Na reaction, the total resonant rate $N_A\langle\sigma v\rangle_R$ is given by the sum of all narrow resonances [16],

$$N_A\langle\sigma v\rangle_R = \frac{1.5399\times10^5}{(\mu T_9)^{3/2}}\sum_i(\omega\gamma)_i e^{\frac{-11.605E_{\rm c.m.,i}}{T_9}}, \quad (4)$$

where T_9 is the temperature in GK ($T_9 = T/10^9$ K), μ is the reduced mass in amu, $(\omega\gamma)_i$ the strength of resonance i in eV, and $E_{\rm c.m.,i}$ is the center-of-mass energy of resonance i in MeV.

The resonance strengths for the 8945 keV doublet are derived using the relation

$$\omega\gamma = \frac{2J+1}{(2j_1+1)(2j_2+1)}\frac{\Gamma_p\Gamma_\gamma}{\Gamma}, \quad (5)$$

where j_1 and j_2 are the spins of the interacting particles i.e., ^{22}Ne and p, and J is the spin of the excited state populated in the compound nucleus, i.e., ^{23}Na. Γ is the total width, i.e., $\Gamma_p + \Gamma_\gamma$. The values of the resonance strengths for the $3/2^+$ and $7/2^-$ state obtained from the present shell model calculations ($\omega\gamma^{\rm SM}$) are compared with the corresponding literature values ($\omega\gamma^{\rm Lit.}$) in Table V. For the $7/2^-$ state, the shell model calculated value is within the limit proposed by Kelly *et al.* [19] and the value of $3/2^+$ is about ≈3 times higher compared to the measured values. Thus, the order of magnitude of the strength values for the $7/2^-$ and $3/2^+$ doublets, deduced from the present shell model calculations, are consistent with the existing data. Unlike the $7/2^-$ state, the strength of the $3/2^+$ state has been very well constrained by various measurements (Table V). In this work, we use the strength value adopted by Williams *et al.* [20] for the $3/2^+$ state and the strength of the poorly studied $7/2^-$ state is determined from the present shell model calculations.

Recently, a new experimental study of the ^{23}Na $+p$ inelastic-scattering reaction at the Q3D magnetic spectrometer at Munich ruled out the earlier reported resonances at $E_x =$ 8862, 8894, and 9000 keV [9]. Hence, these resonances are omitted from the present work. For resonances at $E_{\rm c.m.} = 35$, 178, 417, 458, 610, 632, and 1222 keV, the strength values are also taken from Ref. [20]. The strengths of resonances located between 632 and 1222 keV, and beyond 1222 keV, are adopted from Ref. [13]. The strength values were further divided by the corresponding electron screening enhancement factor, taken from Ref. [20].

The contributions of various individual resonances and the nonresonant component (DC4 + subthres.) normalized to the median STARLIB-2013 rates [13] are shown in Fig. 7(a). At very low temperatures, $T_9 \leqslant 0.05$, the reaction rate is

TABLE V. Resonance strengths of $E_x = 8945$ keV doublets ($3/2^+, 7/2^-$) from the present shell model calculations ($\omega\gamma^{\rm SM}$) compared with literature values ($\omega\gamma^{\rm Lit.}$).

E_x (keV)	$E_{\rm c.m.}$ (keV)	J^π	Γ_p (eV)	$\omega\gamma^{\rm SM}$ (eV)	$\omega\gamma^{\rm Lit.}$ (eV)
8945	151	$3/2^+$	2.88×10^{-7}	5.76×10^{-7}	$(1.9 \pm 0.1) \times 10^{-7}$ [20] $(1.48 \pm 0.1) \times 10^{-7}$ [16] $(1.8 \pm 0.2) \times 10^{-7}$ [17] $(2.2 \pm 0.2) \times 10^{-7}$ [18] $2.03(40) \times 10^{-7}$ [19] $(2.0 \pm 0.5) \times 10^{-7}$ [23] $1.7^{+0.50}_{-0.40} \times 10^{-7}$ [7]
8944	150	$7/2^-$	1.94×10^{-8}	7.77×10^{-8}	$\leqslant 9.2 \times 10^{-9}$ [11] $\leqslant 9.7 \times 10^{-8}$ [19] $(3.93 \pm 0.9) \times 10^{-9}$ [23]

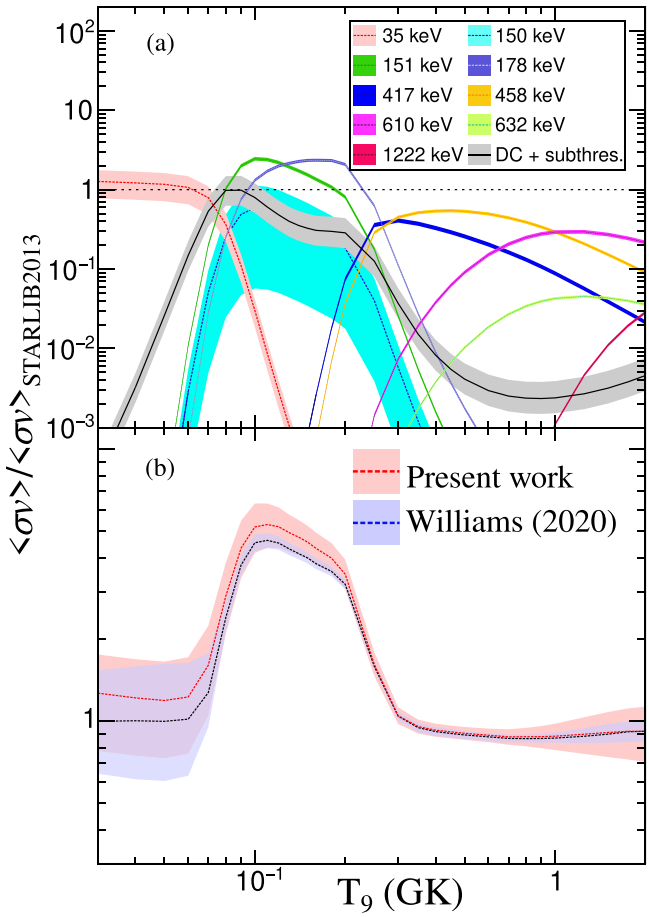

FIG. 7. Reaction rate for the ^{22}Ne$(p,\gamma)^{23}$Na reaction as a function of temperature in GK. (a) Comparison of the individual resonant and nonresonant capture contributions relative to the STARLIB-2013 rate. (b) The total rate from the present work (red) and the measurement by Williams *et al.* [20] (blue) normalized to the STARLIB-2013 rate. The bands correspond to the uncertainties in the rates and the dotted lines represent the mean rates.

dominated by the 35 keV resonance. The temperature range $T_9 = 0.08$–0.1 is significant for the process of hot bottom burning (HBB) in asymptotic giant branch (AGB) stars [18]. In the previous studies by Ferraro *et al.* [18] and Santra *et al.* [23], the 68 and 100 keV resonance had large contributions at these temperatures. However, in this work, these resonances are removed, and the rate is affected by the doublets at 150 keV, the resonance at 178 keV, and the nonresonant capture component. The present nonresonant rate derived from the systematic *R*-matrix calculations is shown with black solid lines and the corresponding uncertainty is shown with the grey band in Fig. 7(a). It is higher at $T_9 = 0.05$–0.1 compared to the earlier rates of Depalo *et al.* [16] and Kelly *et al.* [19], and agrees with the rates of Ferraro *et al.* [18] and Santra *et al.* [23]. The bands in Fig. 7(a) correspond to the uncertainties in the rates, and the dotted lines represent the mean rates. The uncertainties in the individual resonant rates are primarily due to the uncertainties in the resonance strength values, whereas for the nonresonant component the major contribution is the uncertainty in the *S* factor. The uncertainty in the $7/2^-$ doublet at 150 keV is shown with the cyan band. The upper and lower limits of the rate for the $7/2^-$ state are due to the strength values from the present shell model calculations and Ref. [23], respectively (Table V). The mean value (dotted lines in blue) is obtained by taking the average of the upper and lower limits.

The total reaction rate is obtained by adding the resonant and nonresonant capture contributions. In Fig. 7(b), the normalized total rate from the present work (red) is compared to the rate by Williams *et al.* [20] (blue). The rate from Williams *et al.* [20] lies within the uncertainty limits of the rate from the present work. At low temperatures $T_9 = 0.08$–0.1, relevant for the AGB stars, our mean rate (red dotted lines) is ≈15–20% higher than the mean rate of Williams *et al.* [20] (blue dotted lines). The reason behind this increase in rate is twofold. First, Williams *et al.* [20] in their work adopted a constant *S* factor of 60 keV b for direct capture and did not take into account the contribution of the 8664 keV subthreshold resonance. Their measurements were limited in the range of $282 \leqslant E_{\text{c.m.}} \leqslant 511$ keV; as a result they could not observe the rising effect in the *S* factor as seen by Ferraro *et al.* [18]. In the present work, we have included the contribution of the 8664 keV subthreshold resonance in our nonresonant rate calculations. The other important factor is the inclusion of the $7/2^-$ state in the resonant rate calculations. Williams *et al.* [20] used the branching ratio given by Kelly *et al.* [19] to obtain the resonance strength of the $E_x = 8945$ keV state, implying they only considered the $3/2^+$ doublet in their rate calculations. For high temperatures $T_9 = 0.2$–0.25, responsible for classical novae nucleosynthesis, our mean rate coincides with the mean rate of Williams *et al.* [20].

IV. CONCLUSION

The ^{22}Ne$(p,\gamma)^{23}$Na reaction rate is reanalyzed by extracting the ANC of the 8664 keV subthreshold state from FRDWBA analysis of the existing ^{22}Ne$(^3\text{He},d)^{23}$Na transfer reaction data at 15 MeV [24]. The present ANC value of 179.5 ± 19.7 fm$^{-1/2}$ for the 8664 keV state is ≈25% higher compared to the previous study by Santra *et al.* [23]. It satisfies the necessary peripherality checks and is further utilized to carry out *R*-matrix calculations. The astrophysical *S*-factor for DC → 8664 keV using the enhanced ANC value explains the existing data of Gorres *et al.* [21] and Kelly *et al.* [19] within the uncertainty limits but underestimates the data of Rolfs *et al.* [2]. The observed rise in the *S* factor of the capture-to-ground state at low energies is well reproduced from the *R*-matrix calculations. The total nonresonant *S* factor from the present work is in good agreement with the low-energy measurements by Ferraro *et al.* [18] and Williams *et al.* [20].

The proton partial widths for the 8945 keV doublets ($3/2^+$ and $7/2^-$) are deduced from shell model calculations with the code NUSHELLX [31]. The resonance strengths of the $7/2^-$ and $3/2^+$ doublets at $E_x = 8945$ keV, derived from the shell model calculations, are consistent with the order of magnitudes of existing data. As the strength of the $3/2^+$ state is very well constrained from several experimental measurements, the value adopted by Williams *et al.* [20] is used in the present work. For the poorly studied $7/2^-$ state, the strengths obtained

from the shell model and Ref. [23] are used as upper and lower limits, respectively. New high-resolution measurements, with high statistics, are required to firmly determine the properties of the $7/2^-$ state at $E_x = 8945$ keV or to rule out its existence.

The thermonuclear reaction rate evaluated in this work omits the three tentative resonances at $E_x = 8862$, 8894, and 9000 keV. The total reaction rate normalized to the STARLIB-2013 rate [13] is compared to the rate of Williams *et al.* [20]. Incorporating the non-resonant rate from the *R*-matrix calculations, and considering the inclusion of the $7/2^-$ state leads to a noticeable increase in the total rate relative to Williams *et al.* [20]. In the temperature range pertinent to HBB processes ($T_9 = 0.08$–1), the mean rate derived from this work is ≈15–20% higher than that reported by Williams *et al.* [20]. For higher temperatures relevant to classical novae nucleosynthesis ($T_9 = 0.2$–0.25), the mean rate obtained in this study matches with the rate by Williams *et al.* [20].

ACKNOWLEDGMENTS

S.M.A. acknowledges support by the U.S. National Science Foundation under Grant No. PHY-2209429 (Windows on the Universe: Nuclear Astrophysics at FRIB). The authors thank Subinit Roy of the University of Calcutta and Philip Adsley from the Texas A&M University for their useful comments and discussions regarding the manuscript.

[1] J. Marion and W. Fowler, Astrophys. J. **125**, 221 (1957).
[2] C. Rolfs *et al.*, Nucl. Phys. A **241**, 460 (1975).
[3] L. Buchmann and C. Barnes, Nucl. Phys. A **777**, 254 (2006).
[4] F. Käppeler, R. Gallino, S. Bisterzo, and W. Aoki, Rev. Mod. Phys. **83**, 157 (2011).
[5] R. G. Gratton *et al.*, Astron. Astrophys. Rev. **20**, 50 (2012), and references therein.
[6] P. Ventura *et al.*, Mon. Not. R. Astron. Soc. **475**, 2282 (2018).
[7] A. Lennarz *et al.*, Phys. Lett. B **807**, 135539 (2020)
[8] C. Iliadis *et al.*, Astrophys. J. Suppl. Ser. **142**, 105 (2002).
[9] D. P. Carrasco-Rojas *et al.*, Phys. Rev. C **108**, 045802 (2023).
[10] C. Angulo *et al.*, Nucl. Phys. A **656**, 3 (1999).
[11] S. E. Hale, A. E. Champagne, C. Iliadis, V. Y. Hansper, D. C. Powell, and J. C. Blackmon, Phys. Rev. C **65**, 015801 (2001).
[12] C. Iliadis *et al.*, Nucl. Phys. A **841**, 31 (2010).
[13] A. L. Sallaska *et al.*, Astrophys. J. Suppl. Ser. **207**, 18 (2013).
[14] C. Broggini, D. Bemmerer, A. Guglielmetti, and R. Menegazzo, Annu. Rev. Nucl. Part. Sci. **60**, 53 (2010).
[15] F. Cavanna *et al.* (The LUNA Collaboration), Phys. Rev. Lett. **115**, 252501 (2015).
[16] R. Depalo *et al.* (LUNA Collaboration), Phys. Rev. C **94**, 055804 (2016).
[17] F. Cavanna *et al.* (The LUNA Collaboration), Phys. Rev. Lett. **120**, 239901(E) (2018)
[18] F. Ferraro *et al.* (LUNA Collaboration), Phys. Rev. Lett. **121**, 172701 (2018).
[19] K. J. Kelly, A. E. Champagne, L. N. Downen, J. R. Dermigny, S. Hunt, C. Iliadis, and A. L. Cooper, Phys. Rev. C **95**, 015806 (2017).
[20] M. Williams *et al.*, Phys. Rev. C **102**, 035801 (2020).
[21] J. Görres *et al.*, Nucl. Phys. A **385**, 57 (1982).
[22] D. G. Jenkins *et al.*, Phys. Rev. C **87**, 064301 (2013).
[23] R. Santra, S. Chakraborty, and S. Roy, Phys. Rev. C **101**, 025802 (2020).
[24] J. R. Powers *et al.*, Phys. Rev. C **4**, 2030 (1971).
[25] I. J. Thompson, Comput. Phys. Rep. **7**, 167 (1988).
[26] G. G. Kiss *et al.*, Phys. Lett. B **807**, 135606 (2020).
[27] J. Dubois, Nucl. Phys. A **104**, 657-676 (1967).
[28] A. Terakawa *et al.*, Phys. Rev. C **48**, 2775 (1993).
[29] R. E. Azuma *et al.*, Phys. Rev. C **81**, 045805 (2010).
[30] A. Lane and R. Thomas, Rev. Mod. Phys. **30**, 257 (1958).
[31] B. A. Brown and W. D. M. Rae, Nucl. Data Sheets **120**, 115 (2014).
[32] Y. Utsuno, T. Otsuka, B. A. Brown, M. Honma, T. Mizusaki, and N. Shimizu, Phys. Rev. C **86**, 051301(R) (2012).
[33] P. D. Kunz, program DWUCK4 (unpublished).
[34] C. Iliadis, *Nuclear Physics of Stars* (Wiley-VCH, New York, 2007).